

Provided for non-commercial research and education use.
Not for reproduction, distribution or commercial use.



This article appeared in a journal published by Elsevier. The attached copy is furnished to the author for internal non-commercial research and education use, including for instruction at the authors institution and sharing with colleagues.

Other uses, including reproduction and distribution, or selling or licensing copies, or posting to personal, institutional or third party websites are prohibited.

In most cases authors are permitted to post their version of the article (e.g. in Word or Tex form) to their personal website or institutional repository. Authors requiring further information regarding Elsevier's archiving and manuscript policies are encouraged to visit:

<http://www.elsevier.com/copyright>



Contents lists available at ScienceDirect

Earth and Planetary Science Letters

journal homepage: www.elsevier.com/locate/epsl

Seismic anisotropy produced by serpentine in mantle wedge

Haemyeong Jung

School of Earth and Environmental Sciences, Seoul National University, Seoul 151-747, Republic of Korea

ARTICLE INFO

Article history:

Received 17 November 2010
 Received in revised form 13 May 2011
 Accepted 21 May 2011
 Available online 12 June 2011

Editor: L. Stixrude

Keywords:

antigorite
 crystal-preferred orientation
 seismic anisotropy
 mantle wedge
 serpentinite
 subduction zone

ABSTRACT

Trench-parallel seismic anisotropy has been observed in many subduction zones in the upper mantle. In this study, the crystal-preferred orientation (CPO) and seismic anisotropy of natural serpentine from Val Malenco in northern Italy and Punta Bettolina in western Italy are studied. It is found that the [001] axes are aligned subnormal to the foliation but the [010] axes of the serpentine are aligned subparallel to the lineation, which is significantly different from that produced in a recent high-pressure experiment. CPOs of serpentine found herein can be used to explain the trench-parallel seismic anisotropy in a cold mantle wedge for serpentine deformed not only at angles greater than 45° but also at low angles such as in horizontal shear from the surface, indicating the broader implications of the CPO of serpentine for interpreting seismic anisotropy than previously thought. It is also found that seismic anisotropy caused by the CPO of serpentine depends on the degree of serpentinization and flow geometry. The seismic anisotropy increases with antigorite volume fraction. The seismic anisotropy of shear waves is large, i.e., 23–36% for samples with an antigorite volume fraction of 40–93%. Current data suggest that the trench-parallel seismic anisotropy with a delay time of 1–2 s in the forearc mantle wedge can be attributed to the CPO of antigorite having [010] axes aligned subparallel to the flow direction and [001] axes subnormal to the flow plane.

© 2011 Elsevier B.V. All rights reserved.

1. Introduction

Seismic anisotropy is widely observed in the upper mantle and is a powerful tool for interpreting the kinematics and dynamics of flow in the mantle (Long and Silver, 2008; Nicolas and Christensen, 1987; Park and Levin, 2002; Savage, 1999). In particular, trench-parallel seismic anisotropy has been observed in subduction zones worldwide (Fouch and Rondenay, 2006; Long and Silver, 2008; Long and van der Hilst, 2006; Nakajima and Hasegawa, 2004; Park and Levin, 2002; Savage, 1999). Factors that cause trench-parallel seismic anisotropy include mantle flow parallel to the trench associated with slab rollback (Long and Silver, 2008; Russo and Silver, 1994), crystal-preferred orientation (CPO) of wet olivine (Jung et al., 2006; Jung and Karato, 2001; Karato et al., 2008; Kneller et al., 2007, 2008), hydration of sub-vertical fault zones in subducting oceanic plates (Faccenda et al., 2008), CPO of dry olivine under high pressure (Jung et al., 2009a), fluid-filled cracks in subducting slabs (Healy et al., 2009), and CPO of serpentine in a limited condition where serpentine is deformed at angles greater than ~45° from the surface by a dominant slip system (001)[100] (Katayama et al., 2009). However, studies on the CPO of serpentine in nature (Bezacier et al., 2010; Hirauchi et al., 2010; Soda and Takagi, 2010) have been very limited.

Many geological and geophysical observations suggest that mantle wedges in subduction zones are at least partially serpentinized as a result of the dehydration of hydrous minerals in the subducting slabs

(Bostock et al., 2002; Boudier et al., 2010; Brocher et al., 2003; Christensen, 2004; DeShon and Schwartz, 2004; Hyndman and Peacock, 2003; Kamiya and Kobayashi, 2000; Smith, 2010; Tibi et al., 2008). Serpentine is the main hydrous mineral in the upper mantle (Hyndman and Peacock, 2003) and has a strong seismic anisotropy in the P-wave velocity up to $V_p = 46\%$ and S-wave velocity up to $V_s = 66\%$ (Bezacier et al., 2010; Mookerjee and Capitani, 2011; Mookerjee and Stixrude, 2009). In the hydrated forearc mantle, antigorite may play an important role in controlling the fabric development and seismic anisotropy (Bezacier et al., 2010; Hirauchi et al., 2010; Katayama et al., 2009; Kneller et al., 2007; Mainprice and Ildefonse, 2009; Mookerjee and Stixrude, 2009; Ulmer and Trommsdorff, 1995). Therefore, serpentine could play an important role in causing trench-parallel seismic anisotropy in subduction zones. In the present study, this hypothesis was tested by studying the CPO of naturally deformed antigorite serpentine. It is found that antigorite in nature is deformed mainly by a dominant slip system of (001)[010] and it produces strong CPO; these findings can be used to explain both the trench-parallel seismic anisotropy in the mantle wedge in many subduction zones and the puzzling observation of a strong seismic anisotropy in some areas (Long and van der Hilst, 2006; Smith et al., 2001).

2. Sample description and methods

Four serpentinite samples with different amounts of antigorite serpentine were studied (Table 1). Samples VM1 and VM3 were collected from Val Malenco in northern Italy, where Malenco

E-mail address: hjung@snu.ac.kr.

Table 1
Sample descriptions and results.

Sample	Locations in Italy	Ant (%)	Ol (%)	Di (%)	Mgt (%)	CPO of antigorite ^a	Max. Vp (%) anisotropy ^b	Max. AVs (%) anisotropy ^b
VM1	Val Malenco	40	52	5	3	[001] \perp F, [010] // L	23.6	23.2
VM3	Val Malenco	87	8	–	5	[001] \perp F, [010] // L	30.8	34.0
12B	Punta Bettolina	93	5	–	2	[001] \perp F, [010] // L	31.4	36.5
12M	Punta Bettolina	78	4	–	18	[001] \perp F, [010] and [100] // L	25.0	22.8

Ant: antigorite, Ol: olivine, Di: diopside, and Mgt: magnetite.

^a CPO pattern of antigorite was determined based on the pole figures and inverse pole figures in Fig. 2 where F and L represent lineation and foliation, respectively.

^b The P-wave anisotropy (Vp) and S-wave anisotropy (AVs) of antigorite are calculated using the elastic constant of antigorite (Bezacier et al., 2010) and by using software (Mainprice, 1990).

ultramafic rocks constitute the ex-subcontinental mantle portion of the Adria lithosphere (Trommsdorff et al., 1993). Using Malenco serpentinite, several researchers have investigated the stability field of antigorite serpentinite at high-pressure and high-temperature conditions (Ulmer and Trommsdorff, 1995), the dehydration embrittlement of serpentinite as a triggering mechanism for intermediate-depth earthquakes (Jung et al., 2004, 2009b; Jung and Green, 2004), and the deformation microstructures of olivine (Jung, 2009). The serpentinite samples 12B and 12M were collected from Punta Bettolina in western Italy during a field excursion in August 2007. Typical microstructures of these serpentinites are shown in Fig. 1. All the samples show well-defined foliation and lineation along the shape-preferred orientation of the serpentinite and olivine. The mineral phases present in the specimen mainly comprise serpentinite (antigorite), olivine, and a small amount of magnetite and diopside (Table 1). Sample VM1 contains the lowest serpentinite content (40%), and sample 12B contains the highest serpentinite content (93%). Sample 12M contains 78% serpentinite and the highest amount of magnetite (18%). The foliation of each sample was determined from the compositional layering and elongation of olivine and serpentinite, while the lineation was determined from the elongation of olivine, serpentinite, and diopside by performing a grain shape analysis of digitized lines in a plane (Panozzo, 1984). The samples were cut parallel to the lineation (x) and perpendicular to the foliation (z) for microstructure analysis. The CPO of antigorite was measured by performing electron backscattered diffraction (EBSD) (Jung et al., 2006). The EBSD patterns were measured on an SEM JEOL 6380 at the School of Earth and Environmental Sciences in Seoul National University, and the EBSD patterns were analyzed using the HKL Channel 5 software. An accelerating voltage of 20 kV at a working distance of 15 mm was employed for the SEM. At each point, the EBSD pattern was indexed manually to ensure an accurate solution. The CPOs of the serpentinite and olivine were measured for individual grains (n=235–374). The seismic velocity and seismic anisotropy were calculated from the orientation data of the serpentinite (antigorite) and olivine using the elastic constants of antigorite (Bezacier et al., 2010) and olivine (Abramson et al., 1997) and a software program (Mainprice, 1990). Minor phases such as diopside and magnetite were ignored in the calculation of seismic anisotropy.

3. Results

3.1. Crystal preferred orientation (CPO) of antigorite

The CPO of antigorite is shown in pole figures (Fig. 2, left panel). The CPOs of antigorite in samples VM1, VM3, and 12B are all similar. The serpentinite [001] axis is strongly aligned subnormal to the foliation, and the [010] axis is strongly aligned subparallel to the lineation (x). This pattern of CPO is significantly different from the

CPOs of the serpentinite produced by experimentally deformed antigorite (Katayama et al., 2009), wherein the [100] axis is strongly aligned subparallel to the lineation. The CPO of the serpentinite (Fig. 2D) in sample 12M, which contains the highest amount of magnetite (18%), is different from that of the other samples, indicating that the CPO of the serpentinite in sample 12M was probably affected by the presence of large amount of magnetite.

3.2. Inverse pole figure and dominant slip system of antigorite

To infer the dominant slip system that causes the natural deformation in antigorite serpentinite, inverse pole figures were drawn, as shown in Fig. 2 (right panel). The three samples VM1, VM3, and 12B show that the serpentinite [001] axis is aligned normal to the foliation and the [010] axis is aligned subparallel to the lineation, indicating that the dominant slip system of antigorite is (001)[010]. Sample 12M shows that the serpentinite [001] axis is aligned normal to the foliation, but both the [100] and [010] axes are aligned subparallel to the lineation, indicating a mixed slip system of (001)[010] and (001)[100].

3.3. Seismic anisotropy of antigorite

The seismic anisotropy of the P- and S-waves was calculated from the CPO of the serpentinite. Fig. 3 shows the seismic anisotropy in a horizontal flow. The reference frame was changed from the pole figure in Fig. 2 to clearly show the polarization direction of the fast shear wave (Vs1). Because the seismic anisotropy of shear wave splitting is usually plotted on the surface plane, the seismic anisotropy in Fig. 3 is plotted in such a way that the center of the pole figure (z) corresponds to the direction normal to the horizontal plane (foliation) and the E–W direction corresponds to the flow direction (lineation, x). In all the specimens, the P-wave velocity is the fastest in the direction subparallel to lineation (x: flow direction). The P-wave velocity is slow near the center of the plot where the slowest serpentinite [001] axis is aligned subnormal to foliation (center of plots in Fig. 3). For all the specimens, the polarization direction of the fast shear wave (Vs1) is oriented nearly normal to the flow direction (lineation, x) which is shown at the center of the pole figure for Vs1 polarization (Fig. 3). This result is important and can be used to explain the trench-parallel seismic anisotropy in the cold mantle wedge of many subduction zones. Four specimens from two sites showed similar features in the polarization anisotropy of the S-wave (Vs1) regardless of the degree of serpentinitization or composition (Fig. 3 and Table 1).

The effect of the degree of serpentinitization on the magnitude of seismic anisotropy is also shown in Fig. 3. The sample with the lowest serpentinite content (40%, sample VM1) shows the lowest P- and S-wave anisotropy (Vp = 23.6% and AVs = 23.2%), and the sample with the highest serpentinite content (93%, sample 12B) shows the highest P- and S-wave anisotropy (Vp = 31.4% and AVs = 36.5%). The

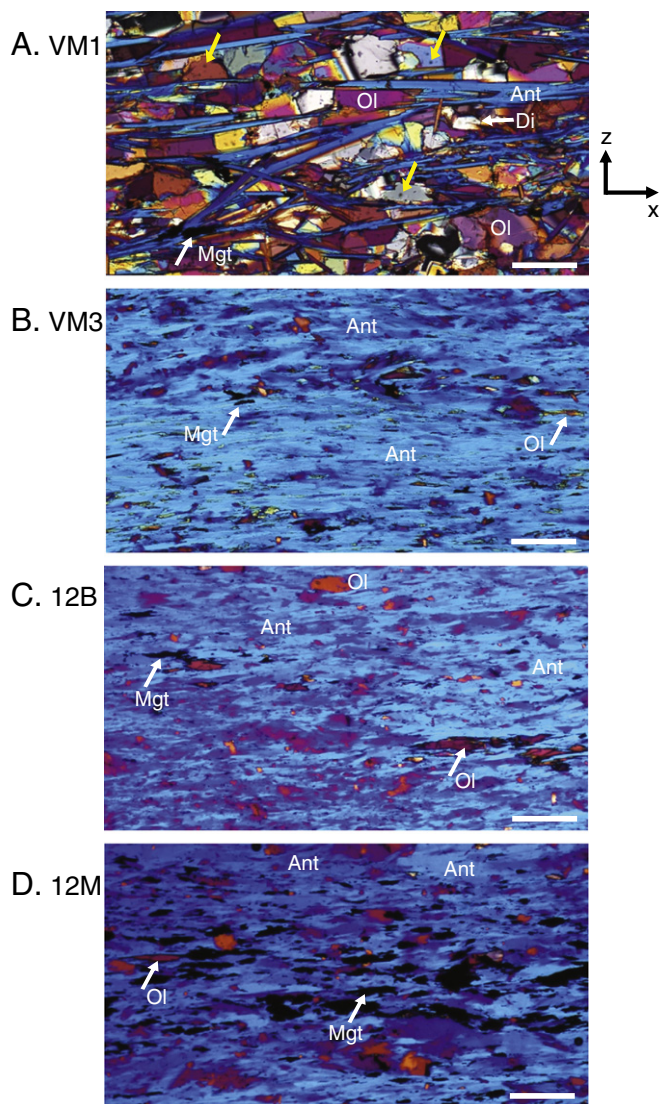


Fig. 1. Optical photomicrographs of samples in cross-polarized light. Typical microstructures of the samples are shown in the X–Z plane (the X-direction is parallel to lineation, and the Z-direction is normal to foliation). All the samples show a strong shape-preferred orientation (SPO) of serpentine. (A, B) Samples VM1 and VM3 are from Val Malenco in northern Italy. (A) The blue elongated minerals are serpentine (antigorite), and most of the other minerals are olivine. The sample consists of 40% serpentine showing an early to middle stage of serpentinization. Small inclusions of serpentine (yellow arrow) are also seen in a large olivine grain. (B) This sample is highly serpentinized (87%) and strongly deformed. Minor olivine and magnetite are visible. (C, D) Samples 12B and 12M are from Punta Bettolina in western Italy. (C) This sample consists of the highest serpentine content (93%), and the SPOs of serpentine, olivine, and magnetite are distinct. (D) This sample consists of 78% serpentine and 18% magnetite. The serpentine and black magnetite grains are elongated subparallel to lineation. Ol: olivine, Ant: antigorite, Di: diopside, and Mgt: magnetite. Scale bars represent 200 μm .

magnitude of the seismic anisotropy produced by the serpentine is much stronger than that produced by the olivine ($V_p = 7.2\%$ and $AV_s = 5.5\%$) in an olivine-dominant specimen collected from the same site (Jung, 2009). The seismic anisotropy produced by the CPO of the serpentine (40% in the sample) is more than three times higher than the seismic anisotropy produced by the CPO of the olivine alone. The magnitude of seismic anisotropy increases with increasing serpentine content in the specimens (Table 1). For sample 12B consisting of 93% serpentine, the seismic anisotropy of S-waves (AVs) is 36% (Fig. 3C). In this case, we need serpentine layers having thickness of only ~13 to 26 km to explain the delay time of 1–2 s for shear wave splitting.

3.4. Effect of dipping angle of serpentine on seismic anisotropy

The seismic anisotropy caused by the CPO of serpentine in a subduction zone may vary with the flow geometry. For example, the dipping angle (θ) of serpentine due to the subduction of the plate may change the seismic anisotropy. Fig. 4 shows the effect of θ on the seismic anisotropy caused by the CPO of the serpentine in the representative sample VM3. The positions of maximum P-wave velocity and V_{s1} polarization change with the increasing dipping angle (θ) of the serpentine. For the vertical propagation of seismic waves shown at the center of the stereonet, the polarization direction of the fast shear wave (V_{s1}) is nearly normal to lineation (flow direction, x) for low dipping angles ($\theta = 0\text{--}10^\circ$), subparallel to the flow direction for intermediate dipping angles ($\theta \cong 30\text{--}45^\circ$), and nearly normal to the flow direction for high dipping angles ($\theta \cong 60\text{--}90^\circ$). Other specimens show similar features for the polarization anisotropy of S-waves, which does not depend greatly on the degree of serpentinization or composition. This result suggests that the trench-parallel seismic anisotropy in the forearc of subduction zones can be attributed to the CPO of serpentine deformed at both angles greater than 45° from the surface and low angles such as in horizontal shear.

3.5. CPO of olivine in partially serpentinized sample (VM1) and its effect on seismic anisotropy

Sample VM1 contains 40% serpentine and 52% olivine. To understand the effect of olivine CPO on the overall seismic anisotropy of specimen VM1, the CPOs of olivine were determined using the EBSD technique (Fig. 5). The olivine [001] axes are aligned subnormal to foliation and the [010] axes are aligned subparallel to lineation, which is called type-EB CPO of olivine. How this type-EB CPO of olivine was formed has not yet been determined experimentally. Further investigation will be needed in the future to understand what caused the type-EB CPO of olivine. By comparing the CPOs of both serpentine and olivine in the same sample (Figs. 2A and 5A), we found that the [010] axes of antigorite are aligned subparallel to the [010] axes of olivine while the [001] axes of antigorite are aligned subparallel to the [001] axes of olivine.

The seismic anisotropy of olivine was calculated as shown in Fig. 5B. Olivine shows P-wave seismic anisotropy of 5.8%, S-wave seismic anisotropy of 4.7%, and polarization directions of fast S-waves are nearly normal to lineation (x) near the center of the pole figure (Fig. 5B, V_{s1} polarization). The seismic anisotropy of the serpentine is shown in Fig. 5C. Antigorite in the specimen with the P-wave seismic anisotropy of 23.6% and S-wave seismic anisotropy of 23.2% shows very high seismic anisotropy, and the polarization directions of the fast S-waves are nearly vertical to lineation (Fig. 5C, V_{s1} polarization), which is similar to that of the olivine. Fig. 5D shows the overall seismic anisotropy for both olivine and antigorite, ignoring minor phases such as diopside (5%) and magnetite (3%). It is found that the overall level of seismic anisotropy decreased because of the addition of the CPO of olivine.

4. Discussion

The current study shows that the CPOs of natural serpentine from Val Malenco in northern Italy and Punta Bettolina in western Italy can be characterized as antigorite [010] axes aligned subparallel to lineation and [001] axes aligned subnormal to foliation, which is in good agreement with the results obtained in previous studies. For example, X-ray diffraction patterns show similar CPO and the same dominant slip system for antigorite from the Piemonte ophiolite nappe of the western Alps, Valtouranche, Italy (Vogler, 1987). Other examples are antigorite from serpentinite mylonite along the Sashu fault, SW Japan (Soda and Takagi, 2010), and antigorite from the

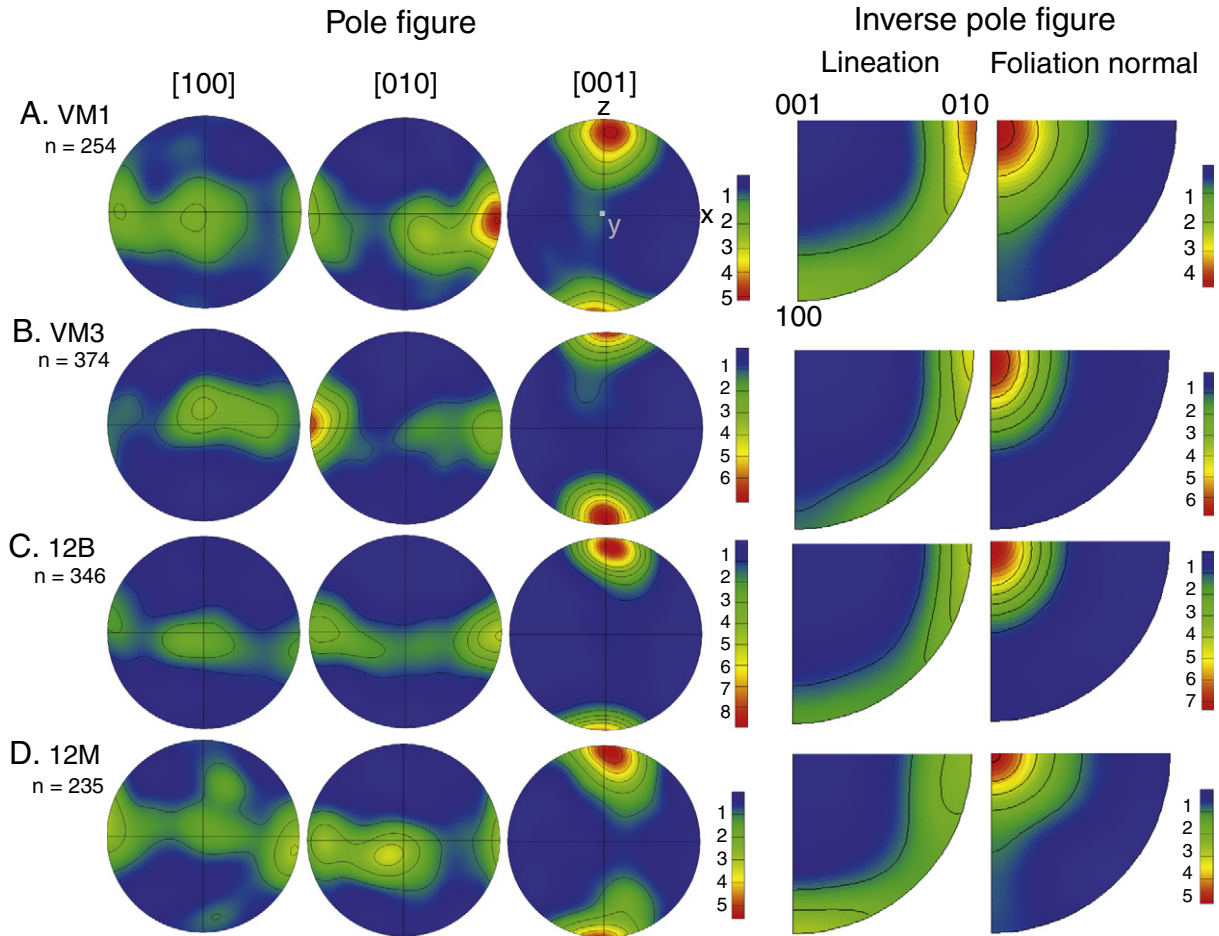


Fig. 2. Pole figures and inverse pole figures of serpentine. Pole figures (left panel) are presented in equal-area and lower-hemisphere projections. The E–W direction corresponds to lineation (x). The N–S direction (z) represents the direction normal to foliation. Inverse pole figures (right panel) corresponding to the pole figures of serpentine (left panel) are presented in two directions: lineation and normal to foliation. The color coding represents the density of the data points. The contours correspond to multiples of a uniform distribution. A half-width of 30° was used to draw both the pole figures and the inverse pole figures. n: number of grains analyzed.

serpentinite shear zone in the Ohmachi Seamount, Izu-Bonin frontal arc (Hirauchi et al., 2010). In contrast, Bezacier et al. (2010) reported a naturally deformed antigorite CPO from Cuba with [100] axes close to lineation. A recent experimental study (Katayama et al., 2009) reported that serpentine is deformed by a dominant slip system of (001)[100]. The reason for the difference in the dominant slip system of serpentine between the natural and experimental samples is not yet clear; the difference may be caused by variations in deformation conditions such as stress, temperature, pressure, strain rate, and strain. If serpentine is deformed by the dominant slip system of (001)[100] such as in the experiment (Katayama et al., 2009), the trench-parallel seismic anisotropy can be explained by the CPO of the serpentine only under very limited conditions where the serpentine is deformed at angles greater than $\sim 45^\circ$ from the surface. A model of the corner flow field in the mantle wedge (Kneller et al., 2008; Long et al., 2007) suggests that a range of orientations from horizontal to highly inclined with foliations is most likely, including all the orientations shown in Fig. 4. Bezacier et al. (2010) argued that various orientations of serpentine deformation are needed to explain the trench-parallel seismic anisotropy in the Ryukyu arc in Japan. The results of the current study show that trench-parallel seismic anisotropy can be attributed to the CPO of serpentine with a dominant slip system of (001)[010] regardless of whether the serpentine is deformed at high angles ($45^\circ < \theta \leq 90^\circ$) or at low angles from the surface ($\theta = 0\text{--}10^\circ$) (Figs. 3 and 4).

Both samples 12B and 12M show similar seismic anisotropy of V_p and V_{s1} polarization (Fig. 3C and D), even though their dominant deformation mechanisms (slip directions) are slightly different. Sample 12B is deformed with a dominant slip system of (001)[010], but sample 12M is deformed with a mixed slip system of both (001)[100] and (001)[010] (refer to the inverse pole figures in Fig. 2). This probably occurs because the seismic velocity along the [001] direction of the serpentine is much slower ($\sim 43\%$) than the velocity along both the [100] and [010] directions (Bezacier et al., 2010), and the difference between the velocities along the two directions ([100] and [010]) is minor ($\sim 3\%$). These results for the seismic anisotropy show that trench-parallel seismic anisotropy can be explained by the CPO of the serpentine developed by either a dominant slip system (001)[010] or a mixed slip system of both (001)[010] and (001)[100].

A TEM study of antigorite schist in the Moses rock from Colorado Plateau (Boudier et al., 2010) has shown a topotactic relationship between antigorite and olivine: (001)ant//((100)ol. Our EBSD study on the CPO of olivine shows the following trend for the orientation relationship between olivine and antigorite: (001)ant//((001)ol (Figs. 2A and 5A). Further study using TEM is required to understand the formation of antigorite in olivine.

The delay times between the fast and slow shear waves vary in the mantle wedges of different subduction zones (Long and Silver, 2008). For example, mantle wedges in Tonga, Aleutians and Ryukyu show long delay times (1–2 s) while mantle wedges in Middle and South

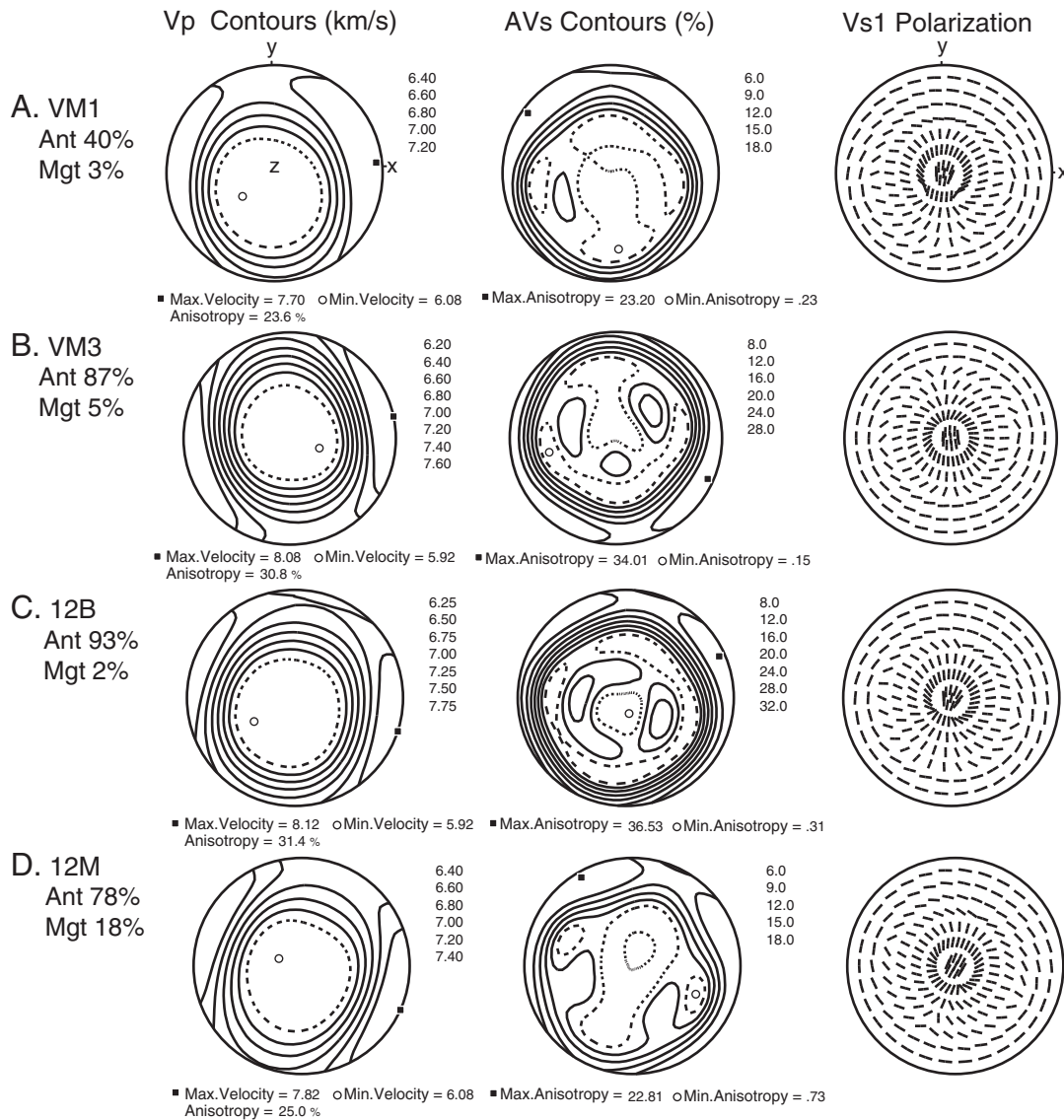


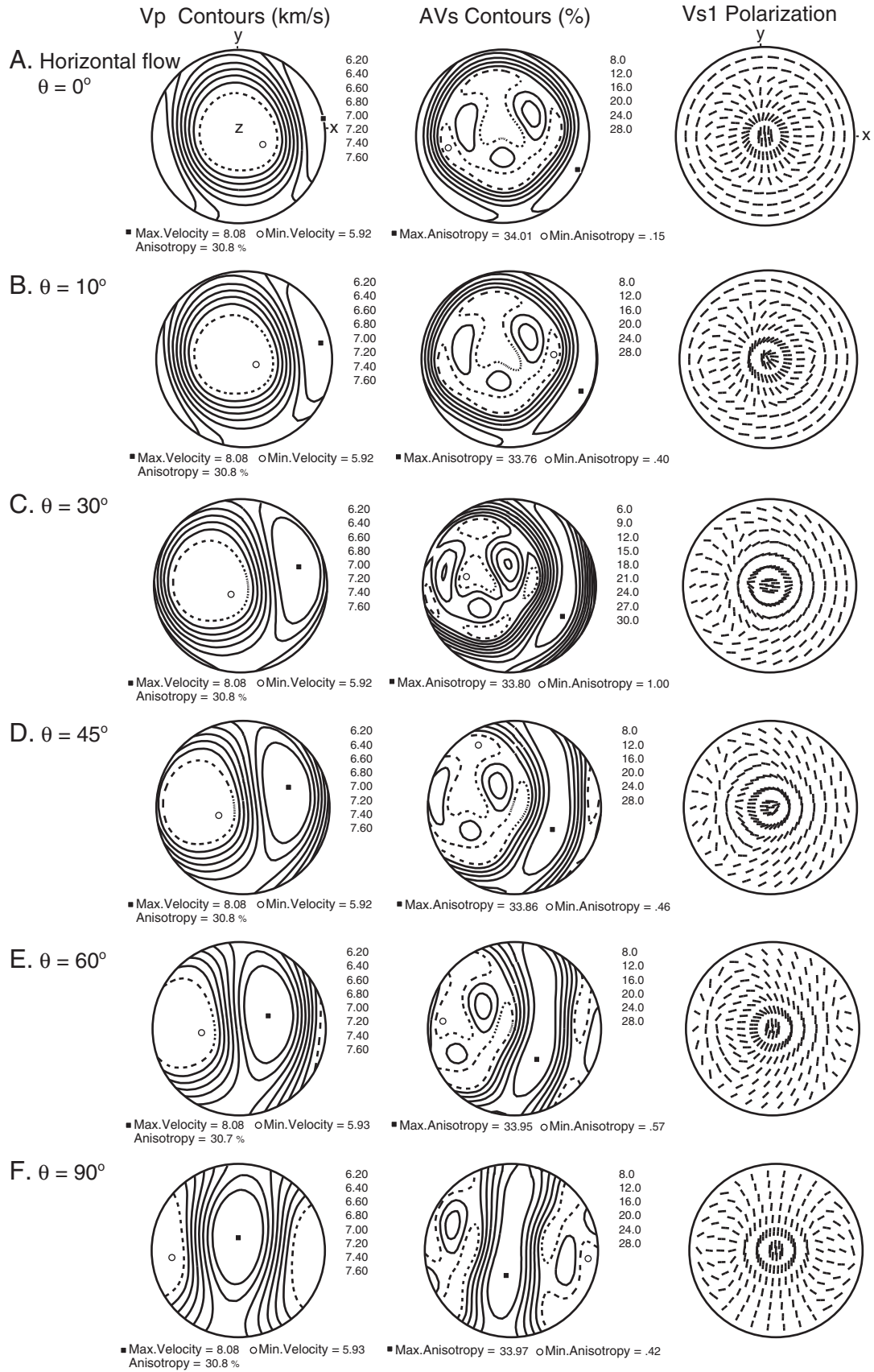
Fig. 3. Seismic anisotropy of naturally deformed serpentine. The effects of the degree of serpentinization and composition on seismic anisotropy are shown in equal-area and lower-hemisphere projections. The seismic anisotropy of serpentine in all the samples is shown in the horizontal flow, where the Y and Z axes are rotated 90° relative to Fig. 2. The X-direction corresponds to the direction of lineation (flow direction). The Z-direction represents the direction normal to foliation (flow plane). The compressional-wave velocity (Vp) and shear-wave anisotropy (AVs) are shown. Vs1 is a plot of the polarization direction of fast S-waves along different orientations of propagation. The center of the stereonet corresponds to vertical propagation. For the vertical propagation of S-waves, the polarization direction of fast S-waves is nearly perpendicular to the flow direction (lineation). Ant: antigorite, Mgt: magnetite.

America and Sumatra show short delay times (up to 0.5 s). Fig. 3 shows that the magnitude of seismic anisotropy caused by serpentine depends on the degree of serpentinization. Based on these data, the long delay times observed in Tonga and Ryuku can be attributed to the large degree of serpentinization in the mantle wedge and the short delay times observed in South America and Sumatra can be attributed to the small degree of serpentinization in the mantle wedge. In addition, if serpentine is deformed at an angle between 10–45° from the surface because of the dipping angle of the subducting slab (Fig. 4), trench-normal anisotropy is produced and this component reduces the total seismic anisotropy in the mantle wedge.

In the Ryukyu mantle wedge, 3-D flow associated with small-scale convection is considered unlikely because most ray paths are confined to the cold corner where high viscosity inhibits free convection (Honda and Saito, 2003). Slab rollback and trench-parallel motion of the overriding plate (Buttles and Olson, 1998; Hall et al., 2000) may produce a trench-parallel flow in the fore-arc mantle. However, these mechanisms are also considered to be unlikely to produce trench-

parallel seismic anisotropy in the Ryukyu subduction system because the slab rollback velocity is low (<1 cm/year) (Heuret and Lallemand, 2005), the curvature in the trench is small, and faults with strike-slip motion are perpendicular to the trench (Kneller et al., 2008). By carrying out geodynamic modeling of the corner flow that incorporates olivine fabric development under wet conditions, Kneller et al. (2008) showed that the B-type fabric of olivine can explain the magnitude and trench-parallel orientation of the deep local-S phases that sample the core of the forearc mantle. However, their calculation (Kneller et al., 2008) showed that the B-type fabric of olivine alone cannot account for the large magnitude of the trench-parallel seismic anisotropy associated with teleseismic phases that sample the shallow cold-tip of the forearc mantle. Highly anisotropic minerals such as antigorite with a strong CPO (b-axis parallel to lineation), as shown in this study, can explain the large trench-parallel seismic anisotropy in the cold-tip of the subduction zone.

In the present study, elastic constants at ambient condition are used to calculate the seismic anisotropy, assuming that they do not



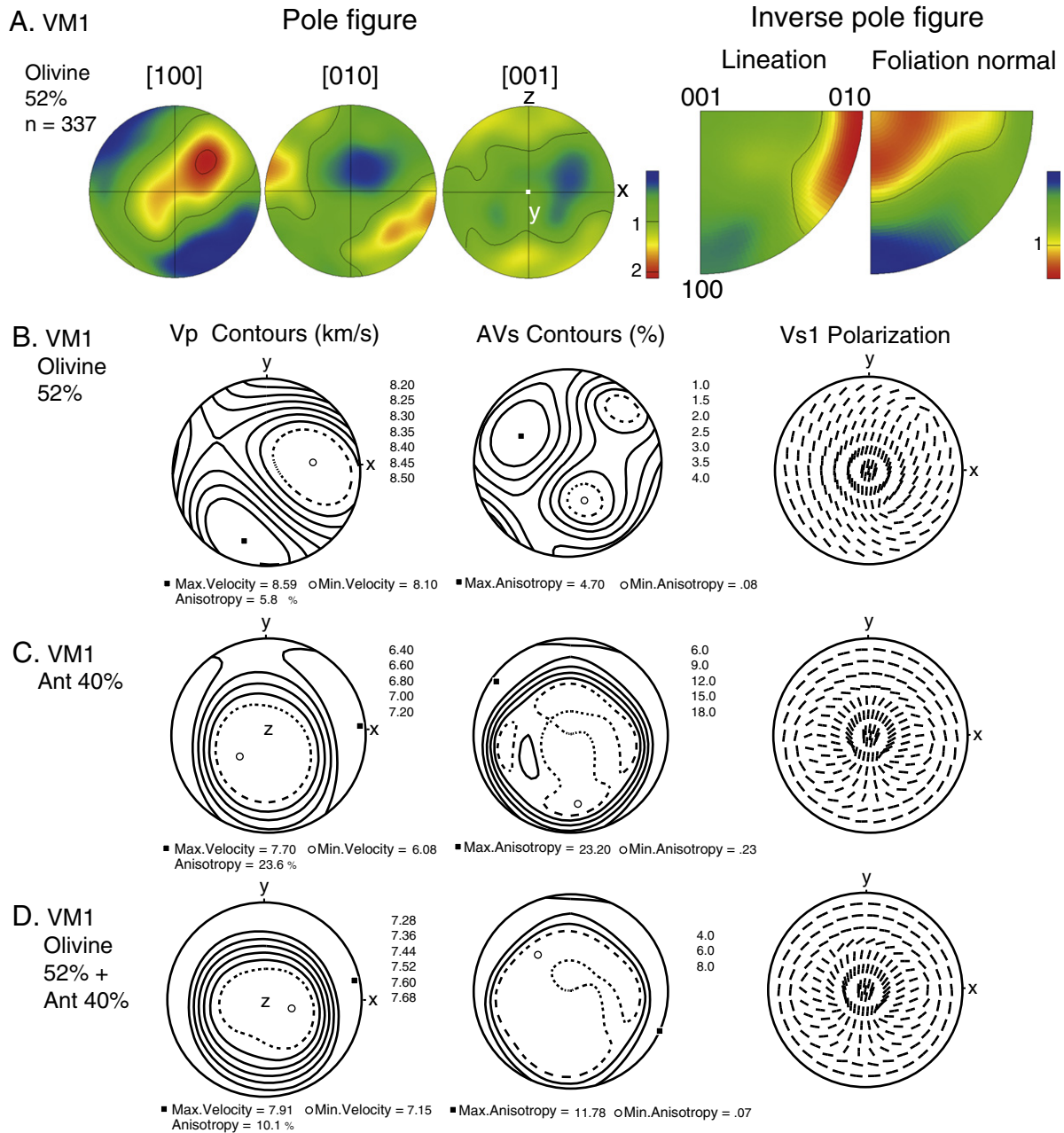


Fig. 5. (A) Pole figure and inverse pole figure of olivine in sample VM1. The pole figure (left panel) is presented in equal-area and lower-hemisphere projection. The E–W direction corresponds to lineation (x). The N–S direction (z) represents the direction normal to foliation. The inverse pole figure (right panel) corresponding to the pole figure of olivine (left panel) is presented in two directions: lineation and normal to foliation. The color coding represents the density of the data points. The contours correspond to multiples of a uniform distribution. A half-width of 30° was used to draw both the pole figure and the inverse pole figure. n: number of grains analyzed. (B) Seismic velocity and anisotropies of P- and S-waves corresponding to pole figure of olivine (Fig. 5A) are shown in equal-area and lower-hemisphere projections. The seismic anisotropy of olivine is shown in the horizontal flow similar to Fig. 3, where the Y and Z axes are rotated 90° relative to Fig. 5A. The X-direction corresponds to the direction of lineation (flow direction). The Z-direction represents the direction normal to foliation (flow plane). The compressional-wave velocity (Vp) and shear-wave anisotropy (AVs) are shown. Vs1 is a plot of the polarization direction of fast S-waves along different orientations of propagation. The center of the stereonet corresponds to vertical propagation. All the other legends are the same as in Fig. 3. (C) Seismic velocity and anisotropies of P- and S-waves corresponding to pole figure of antigorite in same sample (VM1). (D) Combined seismic velocity and anisotropies of P- and S-waves of olivine plus antigorite in sample VM1. Minor phases such as diopside and magnetite are ignored in the calculation. Elastic constants of olivine (Abramson et al., 1997) and antigorite (Bezacier et al., 2010) are used.

Fig. 4. Effect of dipping angle of serpentine (sample VM3) on seismic anisotropy. The plots are shown in equal-area and lower-hemisphere projections. The X-direction corresponds to the direction of lineation (flow direction). The Z-direction represents the direction normal to foliation (flow plane). The seismic anisotropy is calculated using the elastic constants for antigorite (Bezacier et al., 2010). (A) Seismic anisotropy of serpentine in a horizontal flow corresponding to CPO of serpentine (Fig. 2B). (B–F) Effect of dipping angle of serpentine on seismic anisotropy. θ represents the westward dipping angle of the serpentine due to a subducting slab. The compressional-wave velocity (Vp) and shear-wave anisotropy (AVs) are shown for various dipping angles ($\theta = 0, 10, 30, 45, 60,$ and 90°) of the serpentine. Vs1 is a plot of the polarization direction of fast S-waves along different orientations of propagation. The center of the figure corresponds to vertical propagation.

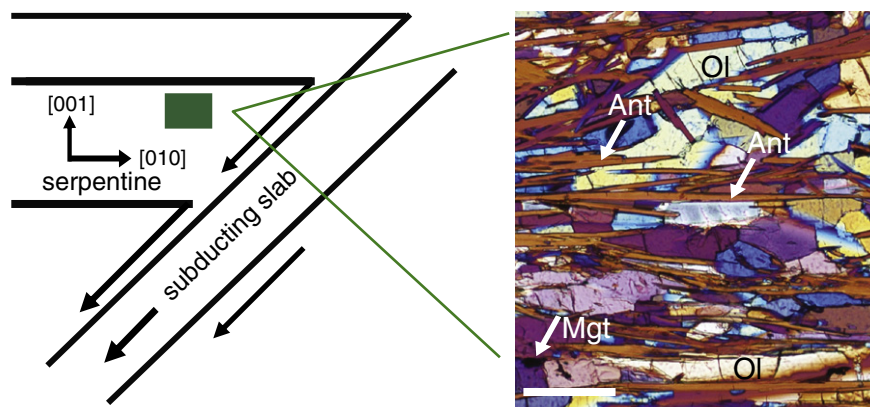


Fig. 6. Schematic diagram of geometry of serpentine fabric in simple corner flow model of material circulation in mantle wedge (left) and optical photomicrograph of sample VM1 in cross-polarized light (right). Ant: antigorite, Ol: olivine, and Mgt: magnetite. Scale bar represents 100 μm .

change at high pressure and high temperature. This is because the elastic constants of antigorite at high pressure and high temperature conditions are not yet known. Serpentine has three polytypes: antigorite, chrysotile, and lizardite. Elastic constants of lizardite have been evaluated at high pressure (Mookerjee and Stixrude, 2009), showing that there is a large effect of Cij's and pressure derivatives on lizardite. Effect of pressure on the elastic constants of antigorite has been recently evaluated (Mookerjee and Capitani, 2011), showing that elastic constants of antigorite can be changed upon compression. However, there are still no data available for the effect of temperature on the elastic constants of serpentine. In the future, seismic anisotropy for given elastic constants of antigorite at high pressure and high temperature would have to be re-evaluated.

In most subduction zones, the mantle wedge is likely to be infiltrated with water and undergo serpentinization (Bostock et al., 2002; Christensen, 2004; DeShon and Schwartz, 2004; Hyndman and Peacock, 2003; Kamiya and Kobayashi, 2000; Tibi et al., 2008). The current study suggests that the serpentine CPO of the flow-parallel [010]-axis maximum can develop in the mantle wedge above the subducting slabs (Figs. 2 and 6). It is notable that the horizontal flow of antigorite (Fig. 3) with a dominant slip system (001)[010] as shown in natural samples in this study can produce trench-parallel seismic anisotropy in the cold forearc mantle wedge in many subduction zones. This also occurs in wet olivine at relatively high temperatures (Jung and Karato, 2001) when the mantle wedge is hydrated by the dehydration of the hydrous minerals in the subducting slabs. Thus, the puzzling observations of the anomalously strong seismic anisotropy (i.e., Ryukyu arc in Japan (Long and van der Hilst, 2006) and Tonga subduction zone (Smith et al., 2001)) also can be explained by the horizontal flow of the antigorite serpentine in the mantle wedge.

5. Conclusions

The CPO of antigorite serpentine was studied in natural specimens from Val Malenco in northern Italy and Punta Bettolina in western Italy. Strong CPOs of antigorite were observed. They are represented by the [010] axes aligned parallel to lineation and [001] axes aligned normal to foliation (Fig. 2), indicating that the serpentine was deformed by a dominant slip system of (001)[010]. The seismic anisotropy caused by the CPO of antigorite has much broader implications for interpreting the trench-parallel seismic anisotropy in the cold mantle wedge than previously thought. For the vertical propagation of S-waves in horizontal shear, the polarization direction of the fast shear wave ($Vs1$) is oriented nearly perpendicular to the flow direction (Fig. 3). Therefore, the CPO of antigorite can be used to explain the trench-parallel seismic anisotropy in mantle wedges in many subduction zones, even though the serpentine is deformed at

low angles from the surface such as in horizontal shear. It is also found that the magnitude of seismic anisotropy caused by the CPO of serpentine strongly depends on the degree of serpentinization and that the polarization anisotropy of the S-waves depends on the flow geometry in the subduction zone (i.e., the dipping angle of the subducting slab).

Acknowledgements

H.J. thanks I. Katayama, B. Reynard, and M. D. Long for the helpful discussions; H. Lim and S. Jung for providing technical support; and D. Mainprice for providing the crystallographic data for the serpentine. Three anonymous reviewers are greatly acknowledged. This work was supported by the Mid-career Research Program through an NRF grant funded by MEST (no. 3345-20100013).

References

- Abramson, E.H., Brown, J.M., Slutsky, L.J., Zaugg, J., 1997. The elastic constants of San Carlos olivine to 17 GPa. *J. Geophys. Res. Solid Earth* 102, 12253–12263.
- Bezacier, L., Reynard, B., Bass, J.D., Sanchez-Valle, C., Van de Moortele, B.V., 2010. Elasticity of antigorite, seismic detection of serpentinites, and anisotropy in subduction zones. *Earth Planet. Sci. Lett.* 289, 198–208.
- Bostock, M.G., Hyndman, R.D., Rondenay, S., Peacock, S.M., 2002. An inverted continental Moho and serpentinization of the forearc mantle. *Nature* 417, 536–538.
- Boudier, F., Baronnet, A., Mainprice, D., 2010. Serpentine mineral replacements of natural olivine and their seismic implications: oceanic lizardite versus subduction-related antigorite. *J. Petrol.* 51, 495–512.
- Brocher, T.M., Parsons, T., Trehu, A.M., Snelson, C.M., Fisher, M.A., 2003. Seismic evidence for widespread serpentinized forearc upper mantle along the Cascadia margin. *Geology* 31, 267–270.
- Buttles, J., Olson, P., 1998. A laboratory model of subduction zone anisotropy. *Earth Planet. Sci. Lett.* 164, 245–262.
- Christensen, N.I., 2004. Serpentinites, peridotites, and seismology. *Int. Geol. Rev.* 46, 795–816.
- DeShon, H.R., Schwartz, S.Y., 2004. Evidence for serpentinization of the forearc mantle wedge along the Nicoya Peninsula, Costa Rica. *Geophys. Res. Lett.* 31.
- Faccenda, M., Burlini, L., Gerya, T.V., Mainprice, D., 2008. Fault-induced seismic anisotropy by hydration in subducting oceanic plates. *Nature* 455, 1097–1100.
- Fouch, M.J., Rondenay, S., 2006. Seismic anisotropy beneath stable continental interiors. *Phys. Earth Planet. Inter.* 158, 292–320.
- Hall, C.E., Fischer, K.M., Parmentier, E.M., Blackman, D.K., 2000. The influence of plate motions on three-dimensional back arc mantle flow and shear wave splitting. *J. Geophys. Res.* 105, 28009–28033.
- Healy, D., Reddy, S.M., Timms, N.E., Gray, E.M., Brovarone, A.V., 2009. Trench-parallel fast axes of seismic anisotropy due to fluid-filled cracks in subducting slabs. *Earth Planet. Sci. Lett.* 283, 75–86.
- Heuret, A., Lallemand, S., 2005. Plate motions, slab dynamics and back-arc deformation. *J. Geophys. Res.* 149, 31–51.
- Hirauchi, K., Michibayashi, K., Ueda, H., Katayama, I., 2010. Spatial variations in antigorite fabric across a serpentinite subduction channel: insights from the Ohmachi Seamount, Izu-Bonin frontal arc. *Earth Planet. Sci. Lett.* 299, 196–206.
- Honda, S., Saito, M., 2003. Small-scale convection under the back-arc occurring in the low viscosity wedge. *Earth Planet. Sci. Lett.* 216, 703–715.
- Hyndman, R.D., Peacock, S.M., 2003. Serpentinization of the forearc mantle. *Earth Planet. Sci. Lett.* 212, 417–432.

- Jung, H., 2009. Deformation fabrics of olivine in Val Malenco peridotite found in Italy and implications for the seismic anisotropy in the upper mantle. *Lithos* 109, 341–349.
- Jung, H., Green, H.W., 2004. Experimental faulting of serpentinite during dehydration: implications for earthquakes, seismic low-velocity zones, and anomalous hypocenter distributions in subduction zones. *Int. Geol. Rev.* 46, 1089–1102.
- Jung, H., Karato, S., 2001. Water-induced fabric transitions in olivine. *Science* 293, 1460–1463.
- Jung, H., Green, H.W., Dobrzinetskaya, L.F., 2004. Intermediate-depth earthquake faulting by dehydration embrittlement with negative volume change. *Nature* 428, 545–549.
- Jung, H., Katayama, I., Jiang, Z., Hiraga, T., Karato, S., 2006. Effect of water and stress on the lattice-preferred orientation of olivine. *Tectonophysics* 421, 1–22.
- Jung, H., Mo, W., Green, H.W., 2009a. Upper mantle seismic anisotropy resulting from pressure-induced slip transition in olivine. *Nat. Geosci.* 2, 73–77.
- Jung, H., Fei, Y.W., Silver, P.G., Green, H.W., 2009b. Frictional sliding in serpentinite at very high pressure. *Earth Planet. Sci. Lett.* 277, 273–279.
- Kamiya, S., Kobayashi, Y., 2000. Seismological evidence for the existence of serpentinitized mantle. *Geophys. Res. Lett.* 27, 819–822.
- Karato, S., Jung, H., Katayama, I., Skemer, P., 2008. Geodynamic significance of seismic anisotropy of the upper mantle: new insights from laboratory studies. *Annu. Rev.* 36, 59–95.
- Katayama, I., Hirauchi, H., Michibayashi, K., Ando, J., 2009. Trench-parallel anisotropy produced by serpentine deformation in the hydrated mantle wedge. *Nature* 461, 1114–1118.
- Kneller, E.A., van Keken, P.E., Katayama, I., Karato, S., 2007. Stress, strain, and B-type olivine fabric in the fore-arc mantle: sensitivity tests using high-resolution steady-state subduction zone models. *J. Geophys. Res.-Solid Earth* 112.
- Kneller, E.A., Long, M.D., van Keken, P.E., 2008. Olivine fabric transitions and shear wave anisotropy in the Ryukyu subduction system. *Earth Planet. Sci. Lett.* 268, 268–282.
- Long, M.D., Silver, P.G., 2008. The subduction zone flow field from seismic anisotropy: a global view. *Science* 319, 315–318.
- Long, M.D., van der Hilst, R.D., 2006. Shear wave splitting from local events beneath the Ryukyu arc: trench-parallel anisotropy in the mantle wedge. *Phys. Earth Planet. Inter.* 155, 300–312.
- Long, M.D., Hager, B.H., de Hoop, M.V., van der Hilst, R.D., 2007. Two-dimensional modelling of subduction zone anisotropy with application to southwestern Japan. *Geophys. J. Int.* 170, 839–856.
- Mainprice, D., 1990. A fortran program to calculate seismic anisotropy from the lattice preferred orientation of minerals. *Comput. Geosci.* 16, 385–393.
- Mainprice, D., Ildefonse, B., 2009. Seismic anisotropy of subduction zone minerals—contribution of hydrous phases. In: Lallemand, S., Funicello, F. (Eds.), *Subduction Zone Geodynamics*, *Frontiers in Earth Sciences*. Springer-Verlag, Berlin Heidelberg, pp. 63–84.
- Mookerjee, M., Capitani, G.C., 2011. Trench parallel anisotropy and large delay times: elasticity and anisotropy of antigorite at high pressures. *Geophys. Res. Lett.* 38, L09315. doi:10.1029/2011GL047160.
- Mookerjee, M., Stixrude, L., 2009. Structure and elasticity of serpentine at high-pressure. *Earth Planet. Sci. Lett.* 279, 11–19.
- Nakajima, J., Hasegawa, A., 2004. Shear-wave polarization anisotropy and subduction-induced flow in the mantle wedge of northeastern Japan. *Earth Planet. Sci. Lett.* 225, 365–377.
- Nicolas, A., Christensen, N.I., 1987. Formation of anisotropy in upper mantle peridotites: a review. *Am. Geophys. Union* 16, 111–123.
- Panozzo, R., 1984. Two-dimensional strain from the orientation of lines in a plane. *J. Struct. Geol.* 6, 215–221.
- Park, J., Levin, V., 2002. Seismic anisotropy: tracing plate dynamics in the mantle. *Science* 296, 485–489.
- Russo, R.M., Silver, P.G., 1994. Trench-parallel flow beneath the Nazca plate from seismic anisotropy. *Science* 263, 1105–1111.
- Savage, M.K., 1999. Seismic anisotropy and mantle deformation: what have we learned from shear wave splitting? *Rev. Geophys.* 37, 65–106.
- Smith, D., 2010. Antigorite peridotite, metaserpentinite, and other inclusions within diatremes on the Colorado Plateau, SW USA: implications for the mantle wedge during low-angle subduction. *J. Petrol.* 51, 1355–1379.
- Smith, G.P., Wiens, D.A., Fischer, K.M., Dorman, L.M., Webb, S.C., Hildebrand, J.A., 2001. A complex pattern of mantle flow in the Lau backarc. *Science* 292, 713–716.
- Soda, Y., Takagi, H., 2010. Sequential deformation from serpentinite mylonite to metasomatic rocks along the Sashu fault, SW Japan. *J. Struct. Geol.* 32, 792–802.
- Tibi, R., Wiens, D.A., Yuan, X.H., 2008. Seismic evidence for widespread serpentinitized forearc mantle along the Mariana convergence margin. *Geophys. Res. Lett.* 35, 6.
- Trommsdorff, V., Piccardo, G.B., Montrasio, A., 1993. From magmatism through metamorphism to sea-floor emplacement of subcontinental Adria lithosphere during pre-alpine rifting (Malenco, Italy). *Schweiz. Mineral. Petrogr. Mitt.* 73, 191–203.
- Ulmer, P., Trommsdorff, V., 1995. Serpentine stability to mantle depths and subduction-related magmatism. *Science* 268, 858–861.
- Vogler, W.S., 1987. Fabric development in a fragment of Tethyan oceanic lithosphere from the Piemonte ophiolite nappe of the western Alps, Valtournanche. *Italy J. Struct. Geol.* 9, 935–953.